RSC Advances

PAPER

View Article Online
View Journal | View Issue

Cite this: *RSC Adv.*, 2024, **14**, 31723

Morphological and molecular control of chemical vapor deposition (CVD) polymerized polythiophene thin films†

Phil M. Smith,‡[a] Laisuo Su, ‡[ab] Yanfei Xu, [c] B. Reeja-Jayan[a] and Sheng Shen *[a]

Oxidative chemical vapor deposition (oCVD) has emerged as one of the most promising techniques for conjugated polymer deposition, especially for unsubstituted polythiophene thin films. oCVD overcomes the insolubility challenge that unsubstituted polythiophene (PT) presents and adds the ability to control morphological and molecular structure. This control is important for enhancing the performance of devices which incorporate organic conductors. In this work, Raman spectroscopy, UV-vis spectroscopy, and AFM reveal that the relative amount of distortion in the polymer chains, the conjugation length and the film roughness are all affected by the CVD deposition conditions, in particular the reactor pressure. PT films deposited at 150 mT and 300 mT are found to have lower chain distortion, longer conjugation lengths and lower surface roughness compared to other deposition pressures. The oCVD PT film is also directly grafted to the trichloro(phenylethyl)silane (PTS) treated substrates, where the effect of PTS grafting is observed to significantly affect film roughness. In addition, we report the first study of the effect of oCVD PT films on the performance of lithium-ion battery electrodes. These oCVD PT films are used to engineer a $LiCoO_2$ cathode in lithium-ion batteries. The observed improvements are a 52% increase in the discharge capacity (67 mA h g^{-1} to 102 mA h g^{-1}) at 10C and a 500% improvement in cycling stability tested at 5C within the voltage range of 3.0–4.5 V (capacity fading rate is reduced from 1.92%/cycle to 0.32%/cycle).

Received 7th September 2024
Accepted 26th September 2024

DOI: 10.1039/d4ra06472k

rsc.li/rsc-advances

1 Introduction

Organic semiconductors, including conjugated polymers, have gained significant attention in both industry and academia due to their potential for lightweight, mechanically flexible applications, which can be further improved with the incorporation of additives, doping, or through structural modifications.[1,2] Technology advancements for integrating organic semiconductors and taking advantage of their unique physical properties have led to a variety of organic electronics, such as organic thin film transistors, organic solar cells and organic light emitting diodes (OLEDS), with an estimated increase of the market size from $46.12 billion in 2019 to $159.11 billion by 2027.[3] Unsubstituted polythiophene (PT) is an important semiconducting polymer because of its simple structure, optoelectronic properties, and high stability.[4] The majority of the existing work related to PT has been focused on substituted PT such as poly(3,4-ethylenedioxythiophene) (PEDOT) and poly(3-hexylthiophene) (P3HT) because of the solubility of their monomers and ease of processing. The insolubility of unsubstituted PT limits its applications as an active layer in devices. Electrochemical polymerization provides an opportunity for depositing PT, however, the substrate requirements are strict in that it must be electrically conducting. Another method is by a simple heat treatment that can be converted to unsubstituted PT.[4] This also places limitations on the type of substrate that can be used.

Oxidative chemical vapor deposition (oCVD) is a vapor phase polymerization technique where all the reactants are in the vapor phase allowing for the deposition of insoluble polymers.[5] Various polymers have been successfully deposited *via* the oCVD technique, such as PT,[6,7] polypyrrole,[8] polyaniline,[9] PEDOT.[10,11] The vapor deposition feature helps generate uniform thin films with controllable thickness for these polymers, which are crucial for applications such as surface engineering and sensor development.[12,13] While there are several studies reporting the deposition of conductive polymers by oCVD, critical gaps exist in understanding the impact of deposition parameters on the morphology and electrical properties of the resulting films.[10] Many conductive polymers can be derived from PT to achieve

[a]*Department of Mechanical Engineering, Carnegie Mellon University, Pittsburgh PA 15213, USA. E-mail: sshen1@cmu.edu*

[b]*Department of Materials Science and Engineering, University of Texas at Dallas, Richardson, TX 75080, USA*

[c]*Department of Mechanical and Industrial Engineering, University of Massachusetts-Amherst, Amherst, MA 01003, USA*

† Electronic supplementary information (ESI) available. See DOI: https://doi.org/10.1039/d4ra06472k

‡ These authors contributed equally to this work.

certain properties. Unsubstituted PT itself also exhibits excellent thermal and environmental stability, high conductivity, tunable electrical and optical properties, and easy processability.[14] Moreover, unsubstituted PT has been successfully deposited with oCVD, using both liquid oxidants like vanadium oxytrichloride[15] and solid-state iron(III) chloride ($FeCl_3$) as the oxidant.[6,7] Therefore, PT is a good candidate to investigate the impact of deposition parameters in oCVD on its morphology and electrical properties.

Here, we study the effect of the deposition pressure on the morphology and molecular structure of unsubstituted PT films deposited using oCVD. Different from the existing study that requires high flow rate (31 sccm) of monomers,[6,7] we explored and optimized the chamber pressure in the low-rate region with $FeCl_3$ oxidant. The low flow rate can help control the thin film uniformity and thickness, and thus is crucial for certain applications. The molecular structure is studied using spectroscopic characterization techniques like Raman and UV-vis, and the morphology is studied using atomic force microscopy (AFM) and scanning electron microscopy (SEM). Furthermore, we investigate the PT film deposition on trichloro(phenylethyl) silane (PTS) treated substrates as compared to untreated substrates. PTS is a silane coupling agent which can be used to bond organic and inorganic materials. Thereby, the PT films graft directly to the PTS treated substrates, which is quite unique to oCVD conjugated polymers.[16–19] To demonstrate the applicability of the oCVD PT, we applied it as a coating on the surface of battery cathode electrode. The coating acts as a physical barrier between reactive electrolytes and the cathode electrolyte, which can eliminate the side reactions between them. In addition, the high conductivity of the PT coating helps the charge rate of the electrode. It is worth noting that applying oCVD polymers for battery application is a novel research direction with little reports.[5] To the best of our knowledge, this is the first report on applying oCVD PT films on the performances of lithium-ion battery electrodes.

The general procedure and oCVD reactor used in this work has been reported by the authors previously.[10,11] The deposition parameters for all the films studied here are identical except for the deposition pressure. This results in different film thicknesses because the deposition process was not optimized for identical film thickness but for monitoring the effect of deposition pressure on the film's morphology and structure. Due to the volatility of the monomer thiophene, heating the monomer jar is not necessary to create vapors, however, the jar temperature was maintained at 30 °C to avoid temperature fluctuations from the room which could alter the monomer flow rate. Previous reports used a total gas flow as high as 31 sccm to promote adsorption of the monomer on the substrate surface.[6,7] Such a high total gas flow would necessitate a high monomer flow rate which is not conducive to smooth films. From our process development for oCVD PT films, using a monomer flow rate of ~1.5 sccm required the stage temperature to be lower than room temperature. A temperature of 10 °C was chosen because it is the lower limit of the system used for all depositions. Typically, when optimizing CVD processes, the ratio of the partial pressure and the saturation pressure of the monomer needs to be determined. However, since the flow rate of the solid oxidant is difficult to determine, this approach could not be used. Instead, post deposition characterizations were done, the deposition parameters were adjusted, and the cycle repeated until the films met the desired requirements. Two types of Si substrates were used for the depositions. In this report the plain untreated Si substrate is referred to as "Plain" and the PTS treated substrate is referred to as "PTS".

2 Experimental

2.1 PTS treated substrate preparation

Bare silicon wafers with native oxide were used as substrates for the trichloro(phenylethyl)silane (PTS) (TCI Chemicals; >98%) treatment. The wafers were first cleaned by sonication in an acetone and then an IPA bath for 5 min each and dried under a nitrogen stream. Hydroxyl groups are formed on the surface of the wafers by exposure to oxygen plasma at 100 W for 10 min in an IPC barrel etcher. The wafers were then placed in an aluminum vacuum chamber with 0.5 mL of the PTS solution. The aluminum chamber was placed on a hot plate at 200 °C and the attachment took place for 2 hours. After 2 hours, the substrates were sonicated in toluene then chloroform and then IPA for 5 min each to remove unattached PTS molecules. This was then followed by drying under a nitrogen stream. These PTS treated substrates were loaded into the oCVD reactor soon after for PT deposition. Untreated bare silicon wafers with native oxide were also used in conjunction with the treated substrates. These untreated substrates were cleaned by sonication in an acetone and then an IPA bath for 5 min each and dried under a nitrogen stream before loading into the oCVD reactor.

2.2 Polythiophene deposition

The monomer, thiophene (Sigma Aldrich; >99%), was placed in a stainless-steel jar outside the CVD reactor and was maintained at a temperature of 30 °C with a heated jacket. A needle valve was used to control the monomer flow at ~1.5 sccm, into the reactor *via* an inlet port. The oxidant, iron(III) chloride ($FeCl_3$) (Sigma Aldrich; anhydrous, >98%), was placed in a heated crucible located within the reactor chamber and heated to 180 °C. The substrates were placed on an inverted heated stage which was set to 10 °C and rotated at 0.5 rpm. The reactor body was maintained at ~65 °C while the gas flow lines were maintained at 30 °C. A range of deposition pressures were used in this work. For the lithium-ion battery work, the deposition pressure was 50 mT. The deposition pressure was selected based on our previous experience that low pressures promote thin and conformal films, which are advantageous for coating the complex and porous surfaces of lithium-ion battery electrodes.[11,13] After the deposition, the films were soaked in methanol for 5 min to remove unreacted monomer and excess oxidant. This step also de-dopes the PT films.

2.3 Material characterization

Raman spectroscopy was done using a Thermo Scientific iXR Raman spectrometer with a 532 nm laser. UV-vis absorption

spectroscopy was done by Josh Stapleton at Penn State University (PSU) with a Cary 5000 Spectrophotometer. AFM was done by Tim Tighe at PSU using a Bruker Dimension Icon in PeakForce Tapping mode. A Scanasyst Air probe (0.4 N m^{-1}, 2 nm nominal tip radius) was used with peakforce setpoints of 0.5–1.25 nN. Images were analyzed in Bruker Nanoscope Analysis. Samples were flattened with a 1st order line fit and the color scale was set to best show the data. The thickness of the films was measured using a Rudolph Ellipsometer AutoEL III. Four points on the sample surface were measured and the average thickness is reported.

2.4 Battery electrochemical characterization

The electrochemical performance was measured in CR2016 coin cells. All the raw materials were purchased from MTI Corporation unless otherwise specified. 80% $LiCoO_2$, 10% polyvinylidene fluoride binder, and 10% super-P conductive agent were mixed in *N*-methyl-2-pyrrolidone. The slurry was then cast onto Al current collectors. After drying in a 110 °C vacuum oven for 12 hours, disks with a diameter of 14 mm were punched and used as cathodes. Coin cells were assembled in a glovebox (Thermo Fisher Scientific) with H_2O and O_2 level less than 0.5 ppm using lithium chip as the anode, Cellgard separator, and ~100 μl of 1 M $LiFP_6$ dissolved in ethylene carbonate/diethyl carbonate (1 : 1 in volume) as the electrolyte. The PT-coated $LiCoO_2$ was rinsed in methanol for 5 min to remove residual monomer and oxidant. The electrochemical performances of coin cells were tested using a VMP3 (Biologic Company) and LAND battery cyclers (LAND Electronics Co., Ltd). All cells were cycled using a C/10 (1C = 145 mA h g^{-1}) rate three times within the 3.0–4.2 V voltage range before conducting other tests. All tests were conducted at room temperature (around 20 °C). The rate capability was measured using the constant–current (CC) constant–voltage (CV) charging protocol followed by CC protocol at different C-rates within 3.0–4.2 V. The current during CC charging is C/3, and the cut-off current during CV charging is C/100. EIS measurement was conducted at 4.0 V (open circuit voltage) for all cells by applying an AC voltage of 10 mV amplitude over the frequency range of 100 kHz to 10 mHz. A high voltage cycling test was carried out within the voltage range of 3.0 V to 4.5 V at 5C using CC protocol for both charging and discharging.

3 Results

The distinguishable peaks in the Raman spectra of PT can be divided into three main regions as shown in Fig. 1. The strongest peaks are seen in region 1 with the peak at ~1500 cm^{-1} corresponding to the asymmetric C=C stretching while the peak at ~1460 cm^{-1} corresponding to the symmetric C=C stretching mode. A shift in the asymmetric C=C peak to lower wavenumbers corresponds to an increase in the conjugation length. On the other hand, the symmetric C=C peak has been shown to be independent of conjugation length.[7,15,20] Table 1 provides the position of the asymmetric C=C peak for samples deposited on plain substrates and PTS substrates at different

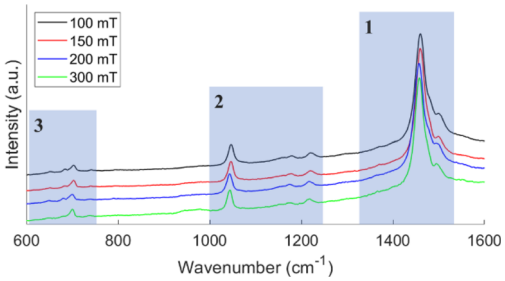

Fig. 1 Raman spectra of oCVD PT films deposited on a plain substrate at different pressures. The three main region for PT films are highlighted by transparent blue boxes.

Table 1 Raman analysis for PT films deposited on plain and PTS substrates

	C=C antisymmetric (cm^{-1})		Distortion ratio	
Pressure (mT)	Plain	PTS	Plain	PTS
100	1499.48	1499.48	0.8791	0.8613
150	1499.48	1498.51	0.8096	0.8165
200	1494.92	1495.88	0.8799	0.8739
300	1494.66	1494.66	0.7971	0.8314

deposition pressure. For the most part, the asymmetric C=C peak shifts to lower wavenumber as the deposition pressure increases, indicating that the film deposited at 300 mT has the highest conjugation length. This holds true for both substrates used. Additionally, at each pressure, the position of the asymmetric C=C peak is very similar for both substrates indicating that the conjugation length is not affected by the different substrates. Region 2 in Fig. 1 contains four distinguishable peaks. The strongest peak located at ~1403 cm^{-1} corresponds to the C–H bending mode while the peak at ~1215 cm^{-1} is assigned to C_α–C_α' linkage vibration between thiophene rings. The remaining two peaks are associated with the distorted parts of the polymer chain often called defect bands.[21] The peaks in the third region show the weakest intensity of all three but is one of the most interesting regions. The peak near ~700 cm^{-1} is assigned to the C–S–C thiophene ring vibration while the peaks at ~652 cm^{-1} and ~680 cm^{-1} are defect bands. The intensity ratio between the defect bands and the C–S–C band (I_{680}/I_{700}) gives a good indicator of the relative amounts of defects or distortion in the polymer chains.[20,22] As seen in Table 1, films deposited at 150 mT and 300 mT demonstrate the lowest amount of chain distortion while films deposited at 100 mT and 200 mT has the highest. Except for the 300 mT film, the relative amount of chain distortion between films deposited on the two different substrates are very similar. These results suggest that films deposited at 300 mT possess the best transport properties due to the relatively larger conjugation length and lower amount of chain distortion.

The Raman spectra of pristine and rinsed films are shown in Fig. 2. The differences seen are indicative of a de-doped film.

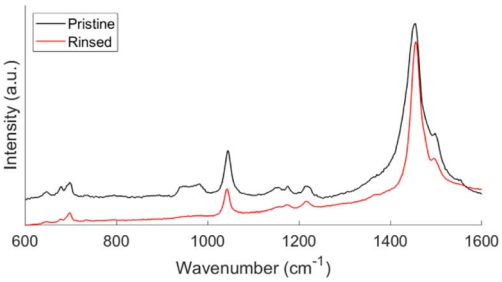

Fig. 2 Raman spectra of pristine and rinsed oCVD PT films. This spectrum represents a film deposited at 150 mT.

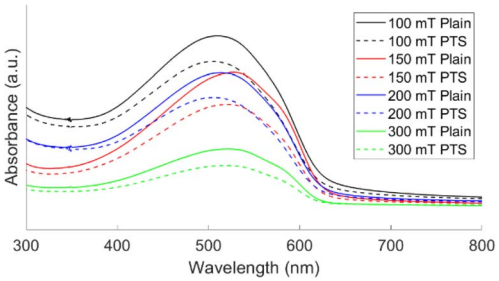

Fig. 3 UV-vis absorption spectra of oCVD PT films deposited on plain and PTS substrates at different pressures.

The rinsed film has narrower and more well-defined peaks compared to the broader peaks seen in the pristine films.[23] The peaks between 900 cm^{-1} and 1000 cm^{-1} correspond to ferric resonances. The disappearance of the peaks after rinsing confirms the removal of unreacted $FeCl_3$ oxidant in the deposited films. The pristine films contain both unreacted monomers and residual oxidants, which causes instabilities in the transport properties.[24,25] Post deposition rinsing improves the transport and physical properties of the film. Like the data discussed from Table 1, the relative distortion ratio as a function of pressure follows a similar trend. However, the actual amount of distortion is greater in the pristine film for reasons previously discussed.

The UV-vis absorption spectra of oCVD PT films deposited on plain and PTS substrates at different pressures are shown in Fig. 3. After rinsing the films, a single pronounced peak is seen. In addition, an absorption shoulder at ~585 nm is observed from all samples. This shoulder has been seen previously in PT films[7,15] and in poly(3-hexylthiophene) (P3HT)[26] films. In P3HT films, this shoulder is a signature of closely packed polymer chains indicating that there is a small degree of ordering in the chains.[27,28] From Table 2, the absorption maxima (λ_{max}) for films deposited at 150 mT and 300 mT are redshifted compared to films deposited at 100 mT and 200 mT. This redshift of λ_{max} is related to an increase in conjugation in the polymer films, which is a well-established relationship from previous work.[29,30] This suggests that the film deposited at 150 mT has the largest conjugation length while the film deposited at 100 mT has the shortest. This result directly contradicts the Raman results where the 300 mT film was predicted to have the largest conjugation length. While Raman spectroscopy can provide information about conjugation length, UV-vis is more sensitive to the conjugation in polymers, as a result, the UV-vis result is more reliable when determining relative conjugation length.[31] Furthermore, Borrelli *et al.* reported higher field effect mobility and channel conductivity for films deposited at 150 mT compared to 300 mT which supports the UV-vis result obtained in this manuscript.[7] Comparing λ_{max} for PT films deposited on plain and PTS substrates, the PT films on the plain substrates have larger conjugation lengths than the PT films on the PTS substrates. This suggests that the transport properties of PT films on the plain substrates will be better.

The optical band gap was determined from the tangent to the band edge or the absorption edge wavelength. The spectrum for the oCVD PT film deposited on a plain silicon substrate at 150 mT, along with the tangent line, is shown in Fig. S1.† The optical band gaps shown in Table 2, are from 1.90–1.94 eV and are in good agreement with those of other oCVD PT films.[6,15,32] The two substrates give identical optical band gaps while the 300 mT sample appear to have the lowest optical band gap. Smaller band gaps are typically correlated to an enhanced conductivity which in conjugated polymers mean longer conjugation length,[33,34] however, the band gap is also sensitive to defects.[35,36] The defects or distortion results from Raman spectroscopy and the conjugation length from UV-vis only paints part of the picture when it comes to understanding carrier mobility in these films. Thermal and electronic characterization of these films will provide a more complete story, this will be explored in a subsequent manuscript.

Table 2 UV-vis analysis of PT films deposited on plain and PTS substrates

	λ_{max} (nm)		Optical band gap (eV)	
Pressure (mT)	Plain	PTS	Plain	PTS
100	511	504	1.92	1.92
150	527	521	1.94	1.92
200	513	506	1.93	1.92
300	521	519	1.90	1.90

We employ atomic force microscopy (AFM) to study the morphology of the prepared oCVD PT thin films. 10 μm × 10 μm AFM scans of the oCVD PT films deposited on plain and PTS substrates at different deposition pressures are shown in Fig. 4. The corresponding 2 μm × 2 μm scans and SEM images are shown in Fig. S2 and S3,† respectively. The morphological features of the resulting PT films in this work are smaller and more well defined compared to the porous morphology previously reported for oCVD PT films deposited using the oxidant $FeCl_3$.[7,37] This is further confirmed by the root mean square (RMS) roughness listed in Table 3. At the same deposition pressure, the morphology and roughness of PT films are visually smoother and smaller than previously reported.[7] This is mainly due to the low substrate temperature during deposition which promotes monomer adsorption and the significantly lower monomer flow rate which promotes the growth of smoother

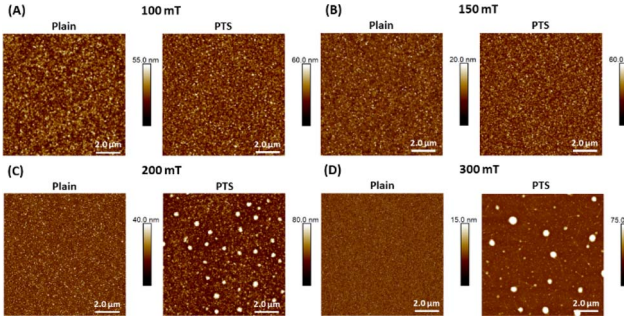

Fig. 4 10 μm × 10 μm AFM scans of oCVD PT films deposited on plain and PTS substrates at different deposition pressures, including (A) 100 mT, (B) 150 mT, (C) 200 mT, and (D) 300 mT.

films.[38,39] As a function of deposition pressure, the film roughness decreases with increasing deposition pressure (Table 3) except for the film deposited at 150 mT which has a lower roughness than the film deposited at 200 mT. Comparing the different substrates, for the most part, the films deposited on the plain substrates have lower roughness values and have lower film thickness. This could be due to non-uniform distribution of binding sites during PTS attachment causing small dense polymer regions as seen in the AFM and SEM images. This, however, does not significantly affect the roughness of the films deposited on the PTS substrates since the roughness is still within an order of magnitude to the films on the plain substrate. As mentioned earlier, only the deposition pressure was adjusted during film growth while all other deposition parameters were held constant. This explains the disparity among the measured film thicknesses. Since the oxidant is kept in the chamber, the deposition pressure would affect the temperature at which the oxidant vaporizes as a result to optimize the deposition for comparable film thickness, the oxidant temperature would also need to be adjusted.

Surface engineering is an effective method to improve the performance of battery electrodes,[40] and oCVD polymers have been proven to be effective at reducing interfacial resistances and promoting charge transport across electrode particles.[11,13] Particularly, the oCVD technique can deposit an uniform coating layer on a complex surface and control the coating thickness on the scale of nanometers. As a proof of concept, we present the effect of a 50 nm oCVD PT film coating on the overall electrochemical performance of $LiCoO_2$ electrodes. The thickness of the films is measured using a Rudolph Ellipsometer AutoEL III.

Table 3 The oCVD PT films deposited on plain Si substrates and PTS substrates

	Roughness (nm)		Film thickness (nm)	
Pressure (mT)	Plain	PTS	Plain	PTS
100	7.1	6.8	214 ± 11.2	218 ± 4.6
150	2.5	6.6	107 ± 2.2	155 ± 3.7
200	4.8	10.7	162 ± 5.0	258.5 ± 11.5
300	1.6	7.3	63 ± 3.6	89 ± 2.3

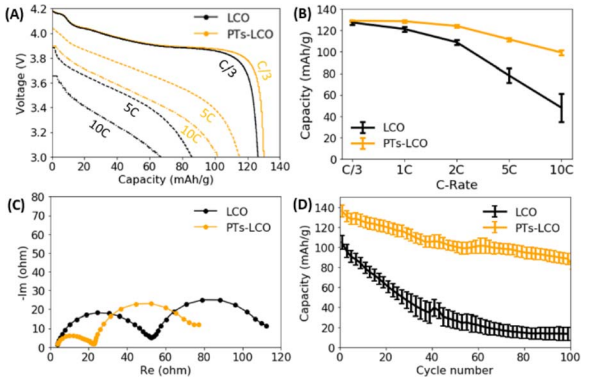

Fig. 5 The effect of oCVD PT coating on the electrochemical performance of $LiCoO_2$. (A) The comparison of discharge curves at different C-rates for the two $LiCoO_2$ electrodes. (B) Statistical comparison of cell capacities (four samples) at different C-rates tested at 3.0–4.2 V. (C) The comparison of electrochemical impedance spectroscopy of the two types of coin cells measured at 4.0 V. (D) Capacity degradation of $LiCoO_2$ electrodes tested at 5C in the voltage range of 3.0–4.5 V.

From our previous study, a ~50 nm thick polymer coating provides the best protection to the $LiCoO_2$ battery electrodes.[13] Fig. 5A compares the discharge curves of the two types of coin cells made from $LiCoO_2$ with and without the PT coating. The PT coating not only increased the discharge capacities, but also promoted the discharge voltages at high rates. For example, the discharge capacity was increased from 67 mA h g^{-1} to 102 mA h g^{-1} at 10C by the PT coating. Fig. 5B further compares the rate capability of $LiCoO_2$ electrodes. The statistical results from four coin cells show that the PT coating significantly improved the rate capability. Compared to the C/3 capacity, the 10C capacity remains 77% in the PT coated $LiCoO_2$ electrodes, while it only remains 37% in the pristine $LiCoO_2$. Fig. 5C compares the electrochemical impedance spectroscopy (EIS) of coin cells with the two different types of the $LiCoO_2$ electrodes. As the same lithium metal was used as the anode for all tested coin cells, the different impedance was contributed from the cathode side. The reduced overall impedance suggests that the PT coating promoted the Li^+ and electron transport at the electrode–electrolyte interface. The increased Li^+ transport kinetics explains the improved rate capability of the $LiCoO_2$ electrode, as shown in Fig. 5A and B. Moreover, Fig. 5D shows that the PT coating largely improved the cycling stability of $LiCoO_2$ electrodes under high current (5C) and high voltage (4.5 V). For example, the capacity fading rate is reduced from 1.92%/cycle to 0.32%/cycle, a 500% improvement, when the specific discharge capacity of the $LiCoO_2$ cathode degraded to 50 mA h g^{-1}. The transport of Li^+ in the PT film can be correlated to the Li^+–polymer binding energy and the number of Li^+ binding sites in the polymer. Small binding energy and sufficient binding sites in the PT film facilitate Li^+ transport in the polymer film.

4 Conclusions

In summary, the morphology and molecular structure of unsubstituted polythiophene thin films were examined as

functions of deposition pressure and substrate type. Films deposited at 150 mT and 300 mT displayed the lowest amount of chain distortion from Raman spectroscopy and the longest conjugation length from UV-vis spectroscopy. UV-vis also revealed that the optical band gap of the 300 mT sample was slightly lower than that of other samples which suggests a more conductivity film. However, further measurement will need to be done to confirm. From the Raman and UV-vis measurements, the type of substrate did not appear to cause significant discrepancies in the results. The morphology of the films was observed to be well defined and the roughness of the films decreased as the deposition pressure increased with the 150 mT sample being the only outlier. Comparing the two types of substrates, the PT films on the PTS substrate were rougher than those on the plain substrate. This may be due to non-uniform distribution of binding sites during PTS attachment. The roughness values report here are also the lowest for PT films deposited using the CVD polymerization technique. At the time of this manuscript preparation, the first report of the effect of oCVD PT coating on $LiCoO_2$ electrodes is reported. An improvement in the discharge capacity, rate capability and cycling life of the battery are all observed from the PT coated electrode when compared to the pristine electrode. These results suggest that oCVD PT coatings can be applied in the development of advanced lithium-ion batteries with fast charging ability and long cycle life.

Data availability

Data for this article, including AFM, Raman, SEM, UV-vis and battery testing data are available at OSF at **https://osf.io/8mn27/?view_only=ab258b5068d54e6cb453c204aa425635**.

Author contributions

S. S. conceived the concept of the work. P. M. S. implemented material synthesis and characterization. L. S. implemented electrodes testing and thickness measurement. B. R.-J. and Y. X. provided additional discussions on the overall ideas. The manuscript was written by P. M. S. and S. S. with comments and input from all authors. S. S. supervised the research. P. M. S. and L. S. contributed equally to this work.

Conflicts of interest

B. R.-J. is the Founder of SeaLion Energy Inc. This CMU spin-out company is commercializing CVD polymerization for energy applications.

Acknowledgements

The authors are grateful to the US National Science Foundation (NSF) under award CMMI-1334630. B. R. J. acknowledges support from US National Science Foundation (NSF) CAREER Award (grant no. CMMI1751605). L. S. acknowledges the New Faculty startup funding provided by the University of Texas at Dallas. The authors acknowledge Joshua Stapleton and Timothy Tighe at Penn State University Material Research Institute for material characterization. The authors acknowledge Xiao Luo for useful discussion and the assistance on manuscript preparation. The authors also acknowledge the Claire & John Bertucci Nanotechnology Laboratory at Carnegie Mellon University (BNL-78657879) for facilitating oCVD deposition and the Material Characterization Facility at Carnegie Mellon University (MCF-677785) for facilitating scanning electron microscopy.

Notes and references

1 S. E. Root, S. Savagatrup, A. D. Printz, D. Rodriquez and D. J. Lipomi, *Chem. Rev.*, 2017, **117**, 6467–6499.
2 W. Zhao, J. Ding, Y. Zou, C. Di and D. Zhu, *Chem. Soc. Rev.*, 2020, **49**, 7210–7228.
3 M. Eslamian, *Nano-Micro Lett.*, 2016, **9**, 3.
4 S. A. Gevorgyan and F. C. Krebs, *Chem. Mater.*, 2008, **20**, 4386–4390.
5 L. Su, S. S. Kumar, A. Manthiram and B. Reeja-Jayan, *Org. Mater.*, 2022, **4**, 292–300.
6 S. Lee, D. C. Borrelli and K. K. Gleason, *Org. Electron.*, 2016, **33**, 253–262.
7 D. C. Borrelli, S. Lee and K. K. Gleason, *J. Mater. Chem. C*, 2014, **2**, 7223–7231.
8 A. Dianatdar, M. Miola, O. D. Luca, P. Rudolf, F. Picchioni and R. K. Bose, *J. Mater. Chem. C*, 2021, **10**, 557–570.
9 Y. Y. Smolin, M. Soroush and K. K. S. Lau, *Ind. Eng. Chem. Res.*, 2017, **56**, 6221–6228.
10 P. M. Smith, L. Su, W. Gong, N. Nakamura, B. Reeja-Jayan and S. Shen, *RSC Adv.*, 2018, **8**, 19348–19352.
11 L. Su, P. M. Smith, P. Anand and B. Reeja-Jayan, *ACS Appl. Mater. Interfaces*, 2018, **10**, 27063–27073.
12 P. Choi, B. S. Parimalam, L. Su, B. Reeja-Jayan and S. Litster, *ACS Appl. Energy Mater.*, 2021, **4**, 1657–1665.
13 L. Su, J. L. Weaver, M. Groenenboom, N. Nakamura, E. Rus, P. Anand, S. K. Jha, J. S. Okasinski, J. A. Dura and B. Reeja-Jayan, *ACS Appl. Mater. Interfaces*, 2021, **13**, 9919–9931.
14 T. P. Kaloni, P. K. Giesbrecht, G. Schreckenbach and M. S. Freund, *Chem. Mater.*, 2017, **29**, 10248–10283.
15 S. Nejati and K. K. S. Lau, *Langmuir*, 2011, **27**, 15223–15229.
16 N. J. Trujillo, M. C. Barr, S. G. Im and K. K. Gleason, *J. Mater. Chem.*, 2010, **20**, 3968–3972.
17 S. G. Im, P. J. Yoo, P. T. Hammond and K. K. Gleason, *Adv. Mater.*, 2007, **19**, 2863–2867.
18 A. Ugur, F. Katmis, M. Li, L. Wu, Y. Zhu, K. K. Varanasi and K. K. Gleason, *Adv. Mater.*, 2015, **27**, 4604–4610.
19 Y. Xu, X. Wang, J. Zhou, B. Song, Z. Jiang, E. M. Y. Lee, S. Huberman, K. K. Gleason and G. Chen, *Sci. Adv.*, 2018, **4**, eaar3031.
20 Y. Furukawa, M. Akimoto and I. Harada, *Synth. Met.*, 1987, **18**, 151–156.
21 M. Fu, G. Shi, F. Chen and X. Hong, *Phys. Chem. Chem. Phys.*, 2002, **4**, 2685–2690.
22 E. A. Bazzaoui, S. Aeiyach, J. Aubard, N. Felidj, P. C. Lacaze, N. Sakmeche and G. Lévi, *J. Raman Spectrosc.*, 1998, **29**, 177–183.

23 M. Akimoto, Y. Furukawa, H. Takeuchi, I. Harada, Y. Soma and M. Soma, *Synth. Met.*, 1986, **15**, 353–360.
24 S. Lee, D. C. Paine and K. K. Gleason, *Adv. Funct. Mater.*, 2014, **24**, 7187–7196.
25 R. M. Howden, E. D. McVay and K. K. Gleason, *J. Mater. Chem. A*, 2012, **1**, 1334–1340.
26 S. Cook, A. Furube and R. Katoh, *Energy Environ. Sci.*, 2008, **1**, 294–299.
27 Y.-J. Huang, W.-C. Lo, S.-W. Liu, C.-H. Cheng, C.-T. Chen and J.-K. Wang, *Sol. Energy Mater. Sol. Cells*, 2013, **116**, 153–170.
28 C. H. García-Escobar, M. E. Nicho, H. Hu, G. Alvarado-Tenorio, P. Altuzar-Coello, G. Cadenas-Pliego and D. Hernández-Martínez, *Int. J. Polym. Sci.*, 2016, **2016**, 1–9.
29 H. Chosrovian, S. Rentsch, D. Grebner, D. U. Dahm, E. Birckner and H. Naarmann, *Synth. Met.*, 1993, **60**, 23–26.
30 P. Frère, J.-M. Raimundo, P. Blanchard, J. Delaunay, P. Richomme, J.-L. Sauvajol, J. Orduna, J. Garin and J. Roncali, *J. Org. Chem.*, 2003, **68**, 7254–7265.
31 W.-F. Su, *Lect. Notes Chem.*, 2013, 89–110.
32 D. C. Borrelli, M. C. Barr, V. Bulović and K. K. Gleason, *Sol. Energy Mater. Sol. Cells*, 2012, **99**, 190–196.
33 J. L. Brédas, *J. Chem. Phys.*, 1985, **82**, 3808–3811.
34 E. Bundgaard and F. C. Krebs, *Sol. Energy Mater. Sol. Cells*, 2007, **91**, 954–985.
35 C. Gong, J. Xiao, L. Zhu, Z. Wang and S. Ma, *Coatings*, 2019, **9**, 570.
36 A. Jadhavar, A. Pawbake, R. Waykar, V. Jadkar, R. Kulkarni, A. Bhorde, S. Rondiya, A. Funde, D. Patil, A. Date, H. Pathan and S. Jadkar, *Energy Procedia*, 2017, **110**, 45–52.
37 S. Lee, D. C. Borrelli, W. J. Jo, A. S. Reed and K. K. Gleason, *Adv. Mater. Interfaces*, 2018, **5**, 1701513.
38 C.-L. Tien, H.-Y. Lin, C.-K. Chang and C.-J. Tang, *Adv. Condens. Matter Phys.*, 2018, **2018**, 1–6.
39 S. Subramani and M. Devarajan, *Mater. Sci.-Pol.*, 2019, **37**, 395–403.
40 L. Su, S. K. Jha, X. L. Phuah, J. Xu, N. Nakamura, H. Wang, J. S. Okasinski and B. Reeja-Jayan, *J. Mater. Sci.*, 2020, **55**, 12177–12190.